Computer Assisted Mechanics and Engineering Sciences, **7**: 321–342, 2000.

Natural convection during ice formation: numerical simulation vs. experimental results

Marilena Giangi[1], Tomasz A. Kowalewski[2], Fulvio Stella[1] and Eddie Leonardi[3]

[1] *Universita di Roma "La Sapienza" Via Eudossiana 18, I-00184 Rome, Italy*

[2] *Institute of Fundamental Technological Research, Polish Academy of Sciences Świętokrzyska 21, 00-049 Warsaw, Poland*

[3] *University of New South Wales, Sydney, Australia 2052*

(Received March 28, 2000)

A numerical and experimental study is presented of unsteady natural convection during freezing of water in a differentially heated cube shaped cavity. A boundary fitted grid as well as the enthalpy–porosity fixed grid numerical models are used in this study. Both numerical models show very good agreement with the experimental data only for pure convection and initial time of freezing process. As time passes the discrepancies between numerical predictions and the experiment became more significant. To elucidate these differences several numerical tests are performed, verifying assumptions made in the models.

1. Introduction

In recent years numerical simulations of phase change problems have attracted much interest due to their significance for several technological processes. The main characteristic of such problems is that a moving interface separates two phases with different physical properties. Melting and solidification are typical examples of phase change problems met in the metallurgical industries or crystal growth technology. These processes involve complex phenomena of mass and heat transfer which determines the quality of the solid phase. The main feature of such problems is the moving interface at which the phase change occurs. Due to the complexity of the problem, application of numerical methods is not a trivial task [4, 22].

It is common in computational fluid dynamics research to validate numerical models against laboratory experiments. In this way it has been possible to design and develop sophisticated aerospace vehicles using numerical models. It may therefore sound peculiar to encounter difficulties in modelling the relatively simple case of solidification with convection in laminar flow. We believe that one of the reasons for this is the physical complexity of such solidification and flow problems, and their sensitivity to the initial and boundary conditions. It is not always appreciated that for such problems, *detailed* knowledge of the experiment is *essential* to correctly define the problem. In this paper we summarise our experiences gained during last few years in matching experimental and numerical results for the simple case of water freezing in a box.

Freezing of water is a very common phase change phenomenon in our environment, and has recently received a lot of attention due to its application to many aspects of human life, such as food processing, organic tissues conservation, water transportation systems and weather prediction. Several heat transfer problems associated with the freezing of water have been reviewed by Fukusako and Yamada [6].

The central problem with modelling phase-change problems is the treatment of the moving solid–liquid interface. Two alternative approaches are used: either transformed or fixed grid methods. In the first method the governing equations are solved for a body-fitted grid which accurately describes the interface. Two sets of equations are solved, one for the liquid and another for the solid phase domain. The phase boundary is tracked in time using the classic Stefan formulation, i.e. balance of heat fluxes at the interface. However, at each time step new grids have to be generated and appropriate transformations of a curvilinear coordinate system calculated. This limits the flexibility of the method and substantially slows down the computations. The fixed grid method, on the other hand, describes the phase change problem using a common set of equations for the whole domain. The heat and mass transfer conditions on the moving interface are incorporated into the governing equations using suitable source terms. The essential feature of the method is the smearing out of the interface, allowing simulation of non-isothermal phase change problems and mushy regions which are present in many practical phase change processes. The question which usually arises is: how do the non-physical modifications of the source term influence the results obtained?

Generally speaking, the application of numerical methods to the practical problem involves a compromise between the complexity of the model (time necessary to solve the problem) and accuracy of the results obtained. Due to the non-linearity of the equations, errors appearing due to inevitable simplifications introduced in the models are difficult to predict and an experimental validation of the results becomes necessary.

The aim of the present work is to verify several assumptions usually used for modelling natural convection and compare the two different approaches, a transformed grid finite differences model [34, 35] and a fixed grid finite volume model [8, 10], by applying them to the problem of water freezing in a cube shaped cavity. A new approach is proposed for the fixed grid enthalpy–porosity model. It improves the simulation by solving the temperature field and the liquid fraction on a refined grid. This permits better resolution of the interface, whilst the time consuming solution of the momentum equation is obtained for a coarse mesh.

The results obtained for both methods are then compared with experimental results obtained for water freezing in the cube-shaped cavity. The full field measurements of the velocity and temperature fields as well as the interface position are used for comparison [18]. Due to the water density anomaly this apparently simple configuration appeared to be a challenging task for numerical simulations. Our previous attempts [1, 2, 3, 10, 15, 19] indicated that the numerical models used need several improvements.

We have used a steady convective flow as the initial conditions for the freezing problem. Hence, in the first part of this paper we compare numerical and experimental results for steady convection without freezing. Several test are performed to investigate the three-dimensionality of the flow, the mesh dependence and effects of the variable properties of the liquid. The effect of finite conductivity of the non-isothermal walls is also discussed.

2. Formulation of the problem

We consider convective flow in a cubic box filled with a viscous heat conducting liquid, which in this case is distilled water. Two opposite vertical walls of the box are assumed isothermal (Fig. 1). One is held at a temperature of $T_c = -10°\mathrm{C}$. Since this is below the freezing temperature of the liquid $T_r = 0°\mathrm{C}$ ice forms on this surface. The opposite vertical wall is held at a temperature of $T_h = 10°\mathrm{C}$. The other four walls which are made from low thermal conductivity material allow the entry of heat from the environment (the air at temperature $T_{\mathrm{ext}} = 25°\mathrm{C}$). The numerical solutions were obtained for Cartesian coordinates with origin placed at a lower corner of the box. The x-axis is horizontal, the y-axis points upwards and the z-axis is parallel to the active vertical plane.

For transient processes uncertainty of the initial conditions may create difficulties in matching experimental and numerical results. In any physical experiment small temperature fluctuations inside the fluid and non-uniformity of temperature at the external walls are inevitable. Hence, to improve our definition of the initial condition, a “warm start” is performed. The freezing starts after a steady convective pattern is established in the cavity. This initial flow state corresponds to natural convection without phase change in the differentially heated cavity, with the temperature

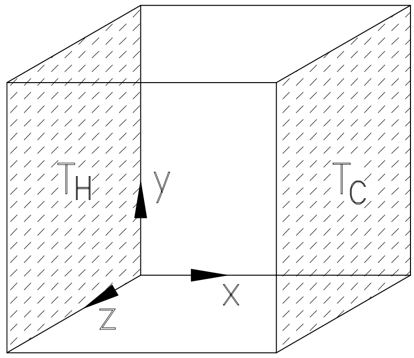

Fig. 1. Physical problem: differentially heated cube shaped cavity

of the cold wall set to $T_c = 0°\text{C}$. The freezing experiment starts, when at time t=0, the cold wall temperature suddenly drops to $T_c = -10°\text{C}$. In the numerical runs, the solution obtained for steady state natural convection was used as the initial flow and temperature fields to start the freezing calculations.

The three dimensionless parameters describing the problem are the Rayleigh number (Ra), Prandtl number (Pr), and Stefan number (Ste), defined as

$$Ra = \frac{g\beta\Delta T H^3}{\nu\alpha}\,, \qquad Pr = \frac{\nu}{\alpha}\,, \qquad Ste = \frac{c\Delta T}{L_f}\,,$$

where $\Delta T = T_h - T_r$ is the difference between hot wall temperature T_h and the interface temperature T_r (melting temperature). In the above definition g, H, α, β, ν, c, L_f, denote the gravitational acceleration, cavity height, thermal diffusivity, coefficient of thermal expansion, kinematic viscosity, specific heat of fluid and latent heat of fusion, respectively.

Due to the non-linear variation of the water density with temperature (Fig. 2) the problem is fully prescribed and the use of a non-dimensional scheme has no particular advantage; it is only used here for comparison purposes. The non-dimensional parameters are defined at the selected reference

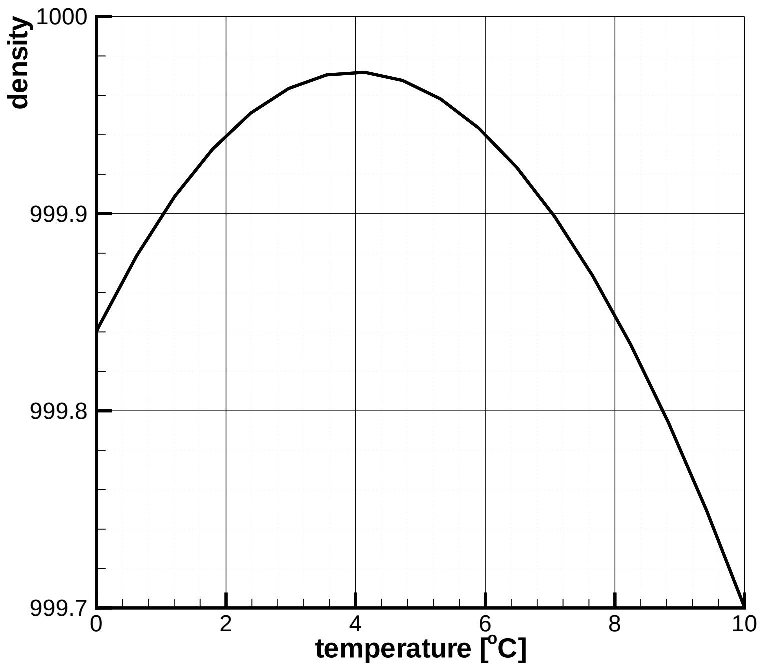

Fig. 2. Variation of water density with temperature close to the freezing point

temperature $T_r = 0°\text{C}$. The corresponding non-dimensional values calculated for a temperature difference $\Delta T = 10$ K, and 38 mm cavity are: $Ra = 1.503 \times 10^6$, $Pr = 13.3$ and $Ste = 0.125$.

A modified Boussinesq approximation has been used, that is a non-linear density variation has been considered but only in the buoyancy term. The density was approximated using a fourth order polynomial obtained by fitting it to the data range of 0°C–20°C given by Kohlrausch [12] (fit error 0.02%):

$$\begin{aligned}\rho = {} & 999.840281 + 0.0673268 \cdot T - 0.00894484 \cdot T^2 \\ & + 8.7846287 \times 10^{-5} \cdot T^3 - 6.6213979 \times 10^{-7} \cdot T^4\end{aligned} \tag{1}$$

where the temperature T is given in degrees Celsius and ρ in kg/m^3.

The expansion coefficient is obtained by differentiating the above formula:

$$\beta = -\frac{1}{\rho}\frac{d\rho}{dT} \,.$$

The remaining physical properties of the liquid, the heat capacity of water (c_l), the thermal conductivity (k_l) and the viscosity ν, are assumed to be functions of temperature as given by Reizes *et al.* [26]. For the temperature range investigated (i.e. from 0°C to 10°C) this resulted in the following variations:

$$\nu = 1.790 - 1.311 \times 10^{-6}\,[\text{m}^2/\text{s}] \tag{2}$$

$$k_l = 0.566 - 0.571\,[\text{W/mK}] \tag{3}$$

$$c_l = 4.202 - 4.186\,[\text{kJ/kgK}] \tag{4}$$

The thermophysical properties of ice were assumed to be constant and equal to: $\rho_s = 916.8$ kg/m^3 for the density, $k_s = 2.26$ W/mK for the thermal conductivity, and $c_s = 2.116$ kJ/kgK for the heat capacity.

During the study of the effects of property variations, when a particular property was taken to be constant it was assumed to be at the reference temperature $T_r = 0°\text{C}$. The latent heat used was $L_f = 335$ kJ/kg.

The thermal conductivity, heat capacity and density of the Plexiglas were measured. When solving the energy equation for the side walls, the values of 0.195 W/mK for the thermal conductivity, and 1.19×10^{-7} m^2/s for the thermal diffusivity were used. The heat transfer coefficient h used for modelling convection heat transfer from the external wall to the surroundings was taken to be 20 W/m^{2}K.

3. Numerical methods

3.1. Vorticity–velocity fixed grid model

A numerical study of freezing water has been conducted on a staggered fixed-grid by using a mathematical formulation based on the enthalpy porosity method [33]. One of the advantages of the fixed grid method is that a unique set of equations and boundary conditions is used for the whole domain, both solid and liquid phase. It allows us to avoid the problem of tracking the solid/liquid interface and the computational cost of grid regeneration.

The governing equations are obtained using averaged quantities [28], yielding the generalised velocity, density, and thermal conductivity defined as:

$$\begin{aligned}\mathbf{v}_m &= f_s \mathbf{v}_s + f_l \mathbf{v}_l \,, \\ \rho_m &= g_s \rho_s + g_l \rho_l \,, \\ k_m &= g_s k_s + g_l k_l \,,\end{aligned}$$

where $\mathbf{v}_l$, $\mathbf{v}_s$, are the velocity of the liquid and solid phase, f_l , f_s , are the liquid and solid mass fraction, g_l , g_s are the liquid and solid volume fraction, ρ_l , ρ_s are the density of the liquid and solid phase. The volume fraction g_l and g_s is related to the mass fraction f_l and f_s via

$$\rho_m f_s = \rho_s g_s \,,$$
$$\rho_m f_l = \rho_l g_l \,.$$

According to the saturated mixture condition the mass and volume fractions must add to unity:

$$f_s + f_l = 1,$$
$$g_s + g_l = 1.$$

Using the assumption that the liquid is Newtonian and incompressible, and that the densities (ρ) and the specific heat (c) in the liquid $(\cdot)_l$ and solid $(\cdot)_s$ phases are equal and constant, the dimensionless governing equations in a vorticity–velocity formulation are:

$$\frac{\partial \mathbf{\Omega}_m}{\partial t} + \nabla \times (\mathbf{\Omega}_m \times \mathbf{v}_m) = Pr\nabla^2 \mathbf{\Omega}_m - RaPr \sum_{i=1}^{N} \gamma_i \nabla \times \left(\theta^i \frac{\mathbf{g}}{|g|} \right) + \nabla \times \mathbf{S} \,, \tag{5}$$

$$\nabla^2 \mathbf{v}_m = -\nabla \times \mathbf{\Omega}_m \,, \tag{6}$$

$$\frac{\partial \theta}{\partial t} + \nabla \cdot (\mathbf{v}_m \theta) = \nabla \cdot \left(\tilde{k} \nabla \theta \right) + B \,, \tag{7}$$

where:

$$\gamma_i = \frac{a_i}{a_1} \Delta T^{(i-1)}$$

and a_i are the coefficients in the density expression (1) and $\Delta T = T_h - T_r$ is the temperature difference of the hot wall T_h and the phase interface temperature T_r . The dimensionless conductivity is defined as

$$\tilde{k} = (1 - f_l) \frac{k_s}{k_l} + f_l$$

such that in the liquid zone ($f_l = 1$) $\tilde{k} = 1$, and in the solid zone ($f_l = 0$) $\tilde{k} = \frac{k_s}{k_l}$.

A Darcy type [28] source term has been adopted in the momentum equation to gradually reduce the velocity in the solidifying zone

$$\mathbf{S} = \frac{-C \,(1 - f_l)^2}{\left(f_l^3 + q\right)} \mathbf{v}_m$$

where C is a large constant value and q is a computational small quantity used to avoid a singularity in solid zone ($\approx 10^{-3}$).

In the energy equation (7) the last term on the right hand side is given by

$$B = -\frac{1}{Ste} \frac{\partial f_l}{\partial t}$$

which takes into account the latent heat due to phase change.

The governing equations (5)–(7) are discretised using a finite volume technique on a staggered grid. A fully implicit scheme has been adopted for the mass and momentum equations, while the temperature field is solved separately in order to evaluate the variation in the local liquid phase fraction. The two linearised algebraic systems are solved using a preconditioned BI-CGStab method [31].

To improve the accuracy of the solution near the phase change front, a refined mesh was used for the temperature. The higher mesh resolution for the energy equation is required since, for water, the thermal boundary layer is thinner then the velocity boundary layer. Hence, the temperature field and the liquid fraction are solved on a refined grid (161×161). This results in better accuracy of the calculated liquid fraction and consequently determination of the phase change interface. The momentum equation is solved using a coarse mesh (41×41).

The velocity field on the finer mesh, necessary for the evaluation of the convection terms in the energy equation, has been obtained evaluating the stream function (ψ) on a 161×161 mesh and then computing the velocity by using the relationship $u = -\frac{\partial \psi}{\partial y}$ and $v = \frac{\partial \psi}{\partial x}$.

At each time step the liquid fraction and the temperature field in eq.(7) are solved using the following iterative procedure. At the time step $n+1$ the iterative fields are initialised to the previous time step n (i.e. θ^*, f_l^*), then the following iterative system, Eqs. (8)–(11), is solved:

$$f_l^i = f_l^{i-1} + Ste\left(\theta^{i-1} - \theta_s\right) \tag{8}$$

subject to the following constraint

$$f_l^i = \max\left[0, \min\left(f_l^i, 1\right)\right], \tag{9}$$

$$f_l^i = f_l^{i-1} + Ste\left(\theta^{i-1} - \theta_s\right), \tag{10}$$

$$Ste\left(\frac{\theta^i - \theta^*}{\Delta t}\right) + Ste\,\nabla \cdot \left(\mathbf{v}_m \theta^i\right) = Ste\,\nabla \cdot \left(\tilde{k} \nabla \theta^i\right) + \frac{f_l^* - f_l^i}{\Delta t}, \tag{11}$$

where i is the index of the iteration level, Δt is the time step, $(\cdot)^*$ indicates the previous time step values and θ_s the phase change temperature. The steps (8)–(11) are repeated until

$$\left\| f_l^i - f_l^{i-1} \right\| < \varepsilon_1 \qquad \text{and} \qquad \left\| \theta^i - \theta^{i-1} \right\| < \varepsilon_2$$

and typically $\varepsilon_1 = \varepsilon_2 = 10^{-8}$ was used.

In the remainder of the paper, the abbreviation FGM is used to indicate results obtained using this fixed grid enthalpy–porosity method.

3.2. Vorticity-vector potential transformed grid model

A modified version of the three-dimensional numerical code FREEZE3D [34] has been used to obtain reference solutions and to perform several test of the model. This finite difference solver of the Navier–Stokes and energy equations can be used to study transient convection with phase change in a fluid with temperature-dependent properties. The governing equations are solved separately for the fluid and solid domain. The governing equations of a Newtonian fluid are those from the physical conservation laws of mass, momentum and energy. The fluid viscosity, thermal conductivity, specific heat and density are functions of temperature. However, the density variation is only applied to the buoyancy term.

In the liquid region the vorticity-vector potential formulation [24] is used. The independent variables are vorticity and the velocity vector potential, thus eliminating need to solve for pressure and continuity. The solenoidal velocity vector field $\mathbf{v}$ can be represented by another solenoidal vector field:

$$\mathbf{v} = \nabla \times \mathbf{\Psi} \tag{12}$$

where $\mathbf{\Psi}$ is the vector potential. Introducing the vorticity vector $\mathbf{\Omega}$,

$$\mathbf{\Omega} = \nabla \times \mathbf{v}, \tag{13}$$

and substituting for $\mathbf{v}$ in terms of $\mathbf{\Psi}$ using (12), we obtain a simple relationship between the vorticity and vector potential

$$\mathbf{\Omega} = -\nabla^2 \mathbf{\Psi}. \tag{14}$$

Using the definition of velocity (12) in the vorticity transport equation (5) one obtains the final form of the three-dimensional set of N–S equation in terms of $(\mathbf{\Omega}, \mathbf{\Psi})$.

In the solid region the energy equation (7) is solved, in which the advection term, $\nabla \cdot (\mathbf{v}_m \theta)$, and the source term, B, are zero.

To couple the solid and liquid regions, two fundamental relations must be satisfied at the interface. Firstly, the temperature at the solid–liquid interface is continuous and equal the temperature of fusion. Secondly, the energy balance including latent heat released at the interface defines the volume of the solid that is formed. This implies the condition for normal velocity of the interface. The governing equations and boundary conditions are solved for a curvilinear coordinate system filling the physical domain. The body fitted grid is smoothed using an elliptic grid generation technique. As the physical domain changes shape, the grid is regenerated at each time step. In solving the time dependent partial differential equations, an Alternating Direction Implicit (ADI) method which marches in time is employed. The vector-potential equation is solved using a successive over-relaxation (SOR) method at each time step. Second order central difference approximation for spatial derivatives and forward difference approximation in time are used. To improve modelling of the physical problem an additional energy equation is solved for the four finite thickness non-isothermal walls enclosing the fluid–solid domain. The physical parameters of the walls and external air temperature are used to solve full conjugate heat transfer problem. The abbreviation ICE3D will be used in the remainder of this paper to indicate results obtained using this model.

4. Experimental

Freezing of distillate water has been investigated experimentally. Water was selected as a flow medium for its well known thermophysical properties and well defined phase change temperature. Our main interest was to collect quantitative information about the phase front position, as well as velocity and temperature distributions at the mid-height vertical plane of the cavity. For this purpose flow images of the centre vertical cross-section were collected at selected time steps for approximately two hours from the onset of cooling. Usually about 100–150 time steps were used. At each time step a series of three to ten RGB images were taken at short time intervals. Special acquisition and image analysis software has been developed and used to obtain 2-D flow pattern (particle tracks) and temperature and velocity fields [1, 11, 15].

The experimental set-up used to acquire the temperature and velocity fields consisted of a convection box, a light source and a 3CCD colour camera. The flow field was illuminated with a 2 mm thin sheet of white light and observed in the perpendicular direction. The colour images comprising of 560×560 pixels were acquired using a 32-bit PCI bus frame grabber. The cube shaped convection box, of 38 mm inner dimension, has two isothermal walls made of aluminium. The four non-isothermal walls were made of 6 mm thick Plexiglas. To avoid water condensation at the side walls, a constant flux of air from a fan was directed onto the cavity. The temperature of the air was 25°C and the speed of air was approx. 3 m/s. The isothermal walls were maintained at a constant temperature using a anti-freeze coolant flowing through attached antechambers. Thermostats controlled the temperature of the cooling and heating liquids. The hot wall temperature was maintained at +10°C. Initially a steady convective flow was allowed to develop for a cold wall temperature of 0°C. The freezing experiment was then started by abruptly opening the inlet valves to the coolant passages. Within about 120 seconds the temperature of the cold wall reaches the prescribed value of −10°C.

Both velocity and temperature fields were monitored using unencapsulated Thermochromic Liquid Crystal (TLC) tracers. Digital evaluation of the tracer images collected for the selected flow cross-section (Digital Particle Image Velocimetry and Thermometry) allowed simultaneous and fully automatic measurements of temperature and velocity 2-D flow fields. Temperature was determined by relating the colour of the tracers to a temperature calibration function ([15, 16, 17]). The 2-D velocity vector distribution has been measured using digital particle image velocimetry (DPIV).

5. Model verification

In previous research [2, 8, 9, 19], it was shown that despite the apparent simplicity of the problem, modelling of freezing water is not an easy task. Small discrepancies between predicted and observed flow structures accumulate as time progresses and eventually result in significant discrepancies between computations and experiments [2, 19]. One possible reason for this is the sensitivity of the investigated flow configuration. Due to the water density anomaly the flow field consists of two competing circulations, which determine the heat flux across the cavity. This flow configuration is highly sensitive to small variations of thermal boundary conditions. It was observed that small modifications of the external heat flux or the temperature range cause extensive changes of the flow pattern (see Fig. 3).

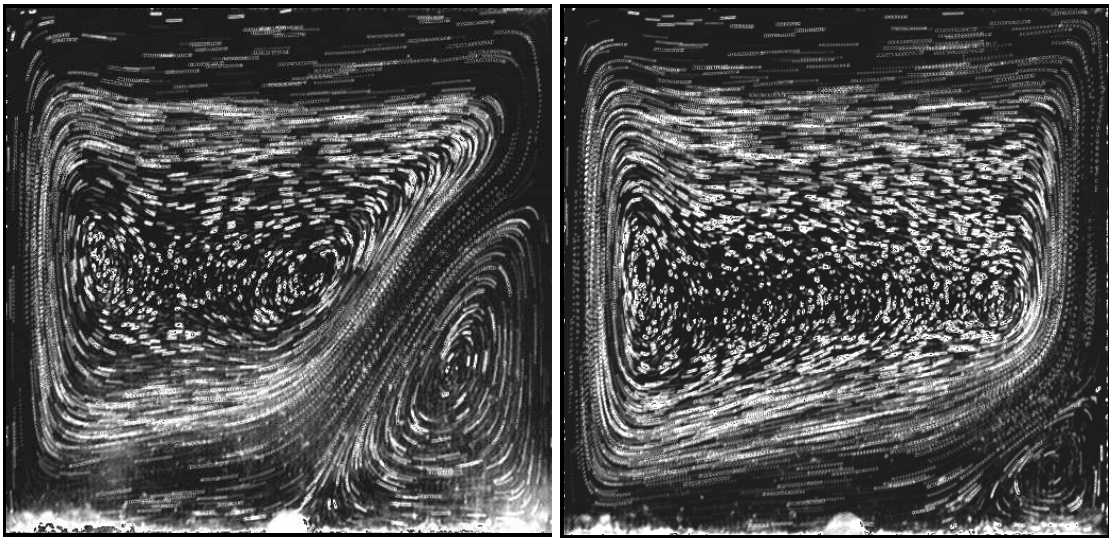

Fig. 3. Natural convection of water observed for $T_h = 10°$C, $T_c = 0°$C; effect of external conditions: left – quiescent external air; right – air flux of 2m/s speed directed on the front wall

This strong non-linearity of the system may also produce unexpected changes in the simulated flow field. On the other hand the cost/accuracy compromise which characterise all computational models forces one to remove all time consuming details not intrinsic to the phenomena investigated. Usually several simplifications have to be introduced to the model to achieve a reasonable computational time, especially when industrial application of the code is sought. Hence, careful analysis of the assumptions introduced in the model seems appropriate. In the following we present several numerical experiments performed to verify the effects of typical simplifications of the model. For this purpose the three-dimensional code ICE3D was mostly used. Its flexibility allows easy manipulation of the different approaches in modifying physical description the problem model. To generate steady state convection a modified version of the false transient solver FRECON3V [29] was used (here referred to as FRE). This pure convection vorticity-vector potential solver has a computational scheme equivalent to the ICE3D code for obtaining solutions to steady state convection. Its robustness and fast convergence helped to speed up the generation of solutions required for the parametric studies undertaken. The compatibility of the numerical solutions of the FRE and ICE3D codes allowed us to use results of the first code as the starting solutions for the freezing problem.

6. Natural convection

Proper modelling of the natural convection of water in the vicinity of the freezing point is essential for the freezing problem. Hence, this configuration was used initially to verify the numerical solutions.

In the experiments the cold wall temperature was set to 0°C, and the hot wall to +10°C. The effects of the density inversion and of the thermal boundary conditions at non-isothermal walls on the flow structures was studied to understand their effect on the final solution and to compare the numerical codes used. A typical flow structure (see Fig. 4) exhibits two recirculation regions, an upper one, where the water density decreases with temperature, and a lower region with an abnormal density variation. Similar flow pattern we found in the numerical solution for the simplified case of the adiabatic boundary conditions [9]. However several discrepancies which were present in the size and location of the recirculation regions indicated the necessity for a more detailed investigation.

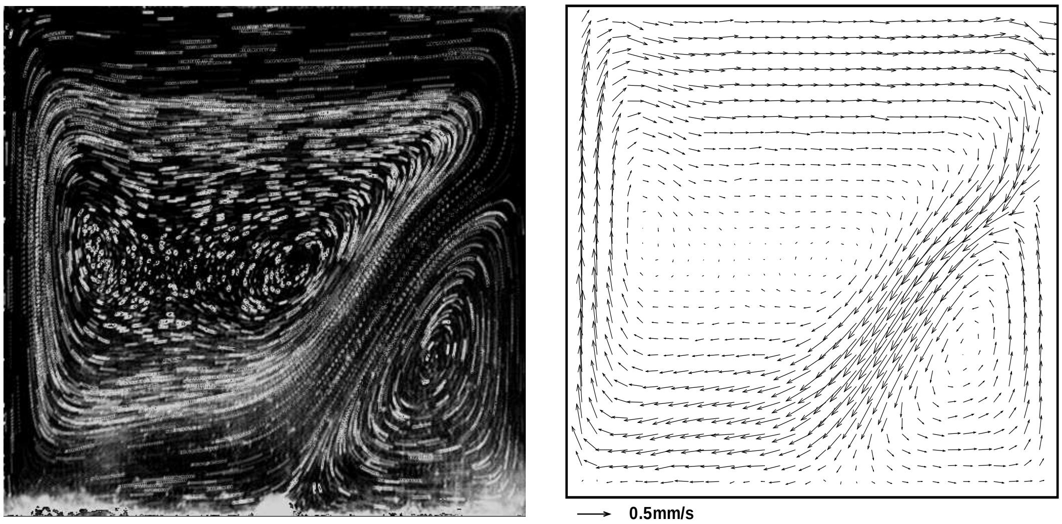

Fig. 4. Natural convection of water observed for $T_h = 10°$C, $T_c = 0°$C; left: flow pattern visualized on multiexposed image of traces; right: evaluated velocity field using PIV technique

In the numerical models used we also consider steady state natural convection of pure water in the freezing cavity with the hot wall kept at a temperature 10°C and the cold wall at a temperature 0°C. When freezing starts, for the fluid domain the ice surface becomes the isothermal boundary at the temperature 0°C. The temperature difference and all effects associated with the water density anomaly remain the same. At early stages of freezing the ice front is parallel to the cold wall and the only difference comparing with pure convection is latent heat released at the phase front. Hence, we believe that most of the conclusions drawn for pure convection apply to the modelling of the initial stages of the freezing problem. Below we describe results of the computational runs performed to test the effects of mesh size, three-dimensionality of the flow, the thermal variation of viscosity, thermal conductivity and thermal capacity of the fluid and the thermal boundary conditions at the passive walls. In most of the cases several cross-sections of the flow were compared to analyse possible differences between solutions. Quantitative comparison can be perfomed by monitoring values of the flow velocity and fluid temperature at a few selected points. For brevity we report only values calculated at three points located along the mid height of the central cross section (ie. $y = z = 0.5$): $x = 0.1,\ 0.5,\ 0.9$. For the investigated configuration these points reflect the main characteristics of the flow. In addition one global parameter, the average Nusselt number calculated at the cold wall, is displayed in the tables. In the table the velocities and temperatures have been non-dimensionalised using a characteristic velocity of α/H (i.e. 3.545×10^{-6} m/s) and characteristic temperature difference of $(T_H - T_C)$ that is 10 K.

6.1. Mesh sensitivity

Mesh sensitivity analysis is an intrinsic aspect of the code verification. In Table 1 five three-dimensional solutions are compared. They are obtained for a uniform mesh with a varying number

Table 1. Mesh dependence test using code FRE, all properties variable, adiabatic boundary conditions, 3D solution

point	$x = 0.1$			$x = 0.5$			$x = 0.9$			
mesh	V_x	V_y	T	V_x	V_y	T	V_x	V_y	T	Nu
21^3	3.18	130	0.633	23.5	2.51	0.662	−60.6	−5.93	0.049	7.40
31^3	−4.89	111	0.596	8.89	5.70	0.634	−51.7	25.5	0.136	7.58
41^3	−7.53	108	0.583	0.927	2.39	0.627	−41.8	47.4	0.160	7.37
61^3	−9.21	107	0.576	−7.12	−2.52	0.623	−35.2	59.7	0.175	7.07
81^3	−9.71	106	0.574	−10.1	−4.45	0.621	−33.3	62.9	0.178	6.94

of grid points from $21 \times 21 \times 21$ to $81 \times 81 \times 81$. Adiabatic temperature boundary conditions (TBC) are set on the non-isothermal walls. All four fluid properties, i.e. density, viscosity, thermal conductivity and heat capacity are assumed to vary with temperature as described earlier. The results are obtained using the false transient code (FRE).

The strong sensitivity of the flow configuration to mesh size variations can be easily seen. Especially in the cold side region of the cavity ($x = 0.9$), the vertical component of velocity changes almost one order of magnitude between the coarse and fine mesh calculations. This effect can be easily understood by noting the flow pattern close to the cold wall (see Fig. 4). Two interacting circulations determine the topology of the flow in this region. A small deviation in their position completely changes the flow configuration, and hence the values of the velocity at the given points. The values presented in the table are mesh point values. The points were selected so that interpolation was not necessary at all grids.

Two straightforward conclusions can be drawn from this test. Firstly, the coarse mesh 21^3 is unacceptable for modelling the flow structure. Secondly, the monitoring of global parameters, such as the Nusselt number does not correctly reflect the accuracy of the calculations, since over the range of meshes considered the change in Nu was less than 10%.

The asymptotic behaviour of the mesh dependence test reveals that a mesh of at least 61^3 is necessary. Even then the variation of velocities at $x = 0.5$ was still significant. Thus the analysis of this problem is computationally expensive in three dimensions.

6.2. Effect of three-dimensionality

In many cases it is justifiable to perform two-dimensional numerical calculations. It substantially reduces the computational effort and permits many solutions to be obtained in a realistic time. However, in the case of the cube shaped cavity three-dimensionality of the flow plays an important role and only the flow in the symmetry plane can be treated as two-dimensional.

The two-dimensional solutions are obtained using the code FRE, with only 5 grid points for the channel depth, with slip kinematic boundary conditions and adiabatic thermal boundary conditions for the side walls to eliminate the flow components in the third direction. These 2D results, generated for the sequence of mesh resolutions from 21^2 to 101^2 are presented in Table 2. As before, adiabatic TBC were assumed for the remaining passive walls and variable fluid properties were used in the code. Hence, these results can be directly compared with the 3D results from Table 1.

First of all it is apparent that 2D simulation also needs a good mesh to guarantee accurate results. Perhaps a mesh of 61^2 can be qualified as one for which results are close to the ideal solution. However, increasing the mesh resolution above this value we may observe still some variation of the velocity values at the centre ($x = 0.5$). It is interesting to note that both the Nusselt number and the temperature field do not depend on the mesh size as much as the velocity does. The same conclusion can be drawn when we compare the 2D solutions with their 3D counterparts reported above.

Except for the most coarse mesh, the 2D solutions are relatively close to their three-dimensional counterparts. However, serious differences between 2D and 3D solutions are always present, especially for the velocity values at the hot wall ($x = 0.1$) and in the centre ($x = 0.5$). It appears in these

Table 2. Mesh dependence test using code FRE from 2D solution; all properties variable, adiabatic boundary conditions

point	$x = 0.1$			$x = 0.5$			$x = 0.9$			
mesh	V_x	V_y	T	V_x	V_y	T	V_x	V_y	T	Nu
21^2	0.252	146	0.642	14.3	1.93	0.665	−53.4	−72.7	0.126	7.05
31^2	−3.96	118	0.596	11.9	5.34	0.629	−51.3	22.1	0.133	7.72
41^2	−6.45	116	0.583	7.57	4.70	0.621	−41.4	45.4	0.158	7.51
61^2	−8.09	115	0.576	2.83	2.42	0.616	−34.7	58.6	0.173	7.21
81^2	−8.58	114	0.574	1.08	1.45	0.615	−33.0	62.0	0.176	7.08
101^2	−8.78	114	0.574	0.311	1.03	0.615	−32.3	63.2	0.178	7.02

regions the heat and mass transfer in the third dimension, across the cavity, cannot be neglected, even for the symmetry plane. It seems that only the temperature field for the 2D solution does not differ significantly from the 3D solution.

6.3. Effect of variable liquid properties

Natural convection in closed cavities are characterised by significant temperature variations within the cavity. Hence, for any physical fluid, variations of its physical properties in space is also inevitable. However, the problem is usually simplified and only the density variation in the buoyancy term is considered in the analytical or numerical models. In the past several authors [20] pointed out that the variation of viscosity, thermal conductivity and thermal capacity of the fluid may have noticeable effect on the flow pattern, leading to the discrepancies between the physical flow and its numerical model, if these variations are not included.

In the case analysed here the temperature range is small and water properties vary relatively little. Therefore, it may appear reasonable to save computational time and ignore the variation of less important fluid properties in the model. Nevertheless, due to the sensitivity of our flow configuration we cannot exclude these small variations, since they may trigger noticeable changes in the flow pattern. To elucidate this effect a few computational runs were performed using the same code (FRE) and the same mesh (41^2), changing modelling of the fluid properties only. The adiabatic TBC are used as well. When constant properties were applied, their value at the reference temperature (0°C) was used in the computations. The results are presented in Table 3.

As expected, the largest effect on the solution was the viscosity variation. For the temperature range investigated the viscosity of water increases by almost 20% at the freezing point. This change reflects in the flow pattern. The effect is clearly visible for the velocity values displayed in Table 3 for the cavity centre ($x = 0.5$) and the cold wall region ($x = 0.9$). Both velocity components significantly change due to the introduction of variable viscosity. Less distinct, but also worth noting, is the change of the temperature field for $x = 0.9$ and of the Nusselt number. These results indicate that whereas the thermal conductivity and the thermal capacity of water can be assumed constant for the small temperature variations, the effect of viscosity variation is important for the simulation of the convection flow with freezing water.

Table 3. Effect of variable fluid properties using code FRE, mesh 41^2 and adiabatic boundary conditions

point	$x = 0.1$			$x = 0.5$			$x = 0.9$			
variable	V_x	V_y	T	V_x	V_y	T	V_x	V_y	T	Nu
ρ, μ, c, k	−6.45	116	0.583	7.57	4.70	0.621	−41.4	45.4	0.158	7.51
ρ, μ	−6.41	115	0.583	7.68	4.67	0.620	−40.4	46.7	0.159	7.50
ρ, k	−6.51	119	0.583	2.56	0.668	0.618	−30.1	60.0	0.173	7.01
ρ	−6.53	119	0.582	2.49	0.462	0.618	−29.4	61.1	0.175	6.98

6.4. Vorticity–velocity fixed grid model

As mentioned above, an improved enthalpy–porosity fixed grid model (FGM) was introduced to speed up the numerical study of freezing water. For convective flows without solidification, the new model differs only in the numerical approach from the previously described vorticity-vector potential model. However, the staggered grid used in this model will result in more accurate solutions at the same grid points. For simplicity the two-dimensional version of the code was used. Also variation of the fluid properties with the temperature is neglected. As in the previous cases, the non-linear density variation has been considered only in the buoyancy term.

Table 4 presents two-dimensional solutions obtained using the FGM model. A staggered uniform mesh was changed from 21×21 to 101×101 points. The adiabatic TBC are set at the non-isothermal walls. These results can be compared with the previous results obtained at the same grid points. However, due to the staggered grid the displayed values are obtained by interpolation (arithmetic mean) to match the same coordinates.

The results show the relatively quick convergence of the code to the asymptotic fine mesh results. Even at the 31^2 mesh, the results are within 10% of the 101^2 mesh. The staggered grid and the vorticity–velocity formulation are superior in conserving the mean vorticity as prescribed by the Stokes theorem. Furthermore this form for the convective terms reduces numerical instabilities. As seen in Table 4 a substantially reduced number of the mesh points generates the accurate solution. Several differences in the velocity values can be encountered when comparing this results and the results generated using FRE code (Table 3). It seems that these differences are rather due to the interpolation errors of the values obtained for the staggered grid. In fact, when velocity profiles or isotherms are compared results produced by these two codes overlap.

Table 4. Mesh dependence for the FGM model, temperature dependent density only ($\rho(T)$), 2D solution for adiabatic boundary conditions

point	$x = 0.1$			$x = 0.5$			$x = 0.9$			
mesh	V_x	V_y	T	V_x	V_y	T	V_x	V_y	T	Nu
21^2	−10.7	106	0.564	−36.7	−40.7	0.594	−15.4	73.7	0.202	7.52
31^2	−8.54	107	0.577	−7.19	−6.49	0.614	−26.2	61.9	0.182	7.02
41^2	−8.25	110	0.577	−6.56	−6.02	0.615	−26.5	65.1	0.182	6.79
61^2	−8.32	113	0.576	−6.47	−5.77	0.614	−25.1	69.1	0.185	6.62
81^2	−8.38	114	0.575	−6.49	−5.70	0.614	−24.5	70.7	0.187	6.55
101^2	−8.41	115	0.575	−6.51	−5.68	0.614	−24.1	71.5	0.187	6.52

6.5. Thermal boundary conditions

The computational models have to be adapted to simulate as closely as possible the physical experiment. The main problem which arises in the simulation of the experimental conditions is a proper definition of the thermal boundary conditions (TBC). In our study the two opposite vertical walls were isothermal. The other four walls were made of plexiglas, and it was assumed that they were adiabatic. Our previous studies [14, 21] indicated that such an assumption may lead to severe deviations of the numerical results from reality. Hence, two approaches were employed to model the boundary conditions on the non-isothermal walls. In the first (referred to as 1-D TBC), heat transfer theory was applied to the side walls modelled as thick, infinitely wide plane plates of uniform conductivity exposed to an external unlimited environment. A specific heat transfer coefficient on each of these surfaces of the box was imposed in the calculations and the heat flux through the walls calculated from the available data on temperature, wall thickness and thermal properties. It was previously found that such an approach to the TBC may still not be sufficiently accurate, if fine structures of the flow are of the interest. This is due to the neglect of the heat transfer along the wall. Hence, in the second approach, three-dimensional conduction in all walls bounding the flow in the computational domain was also incorporated, i.e. a coupled solid–fluid conjugate heat transfer problem is solved (2-D TBC). The accuracy of modelling the TBC depends for this case mainly on the proper estimation of the heat transfer coefficient at the external surfaces of the walls.

For the investigated cases the observed flow pattern appears to be very sensitive to the TBC formulation. Figure 5 illustrates the difference of the simulated flow pattern for adiabatic and constant heat flux TBC at the passive walls. The upper clockwise circulation transporting hot liquid towards the top wall, grown in size for the last case, completely changing the position of the saddle point, i.e. where it meets the lower counter-clockwise circulation. This explains the sensitivity of the pattern observed in the experiments (see Fig. 3). In Fig. 6 vertical velocity profiles extracted along the cold wall illustrate this strong dependence of the saddle point position on the heat flux through the side walls.

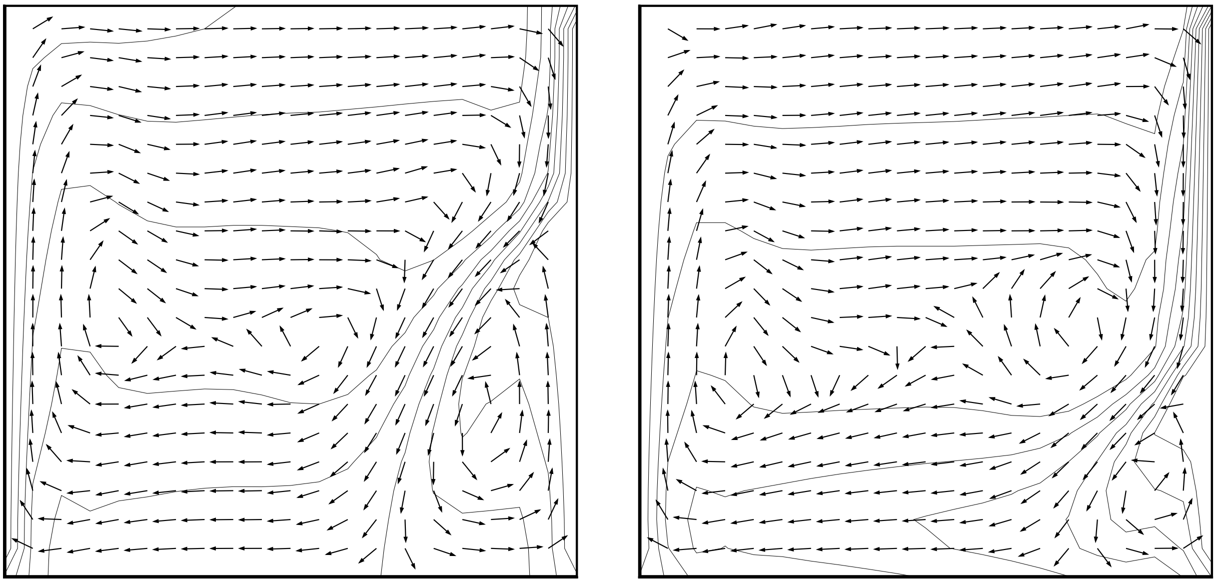

(a) (b)

Fig. 5. Natural convection of water, 3D numerical results (FRE) for $Th = 10°$C, $Tc = 0°$. Velocity and temperature fields in the centre plane ($z = 0.5$). Effect of TBC; (a) – adiabatic TBC, (b) – non-adiabatic 1D-TBC with heat transfer coefficient $h = 40$ W/Km^2

It was concluded that proper modelling of the TBC is of great importance for the freezing water problem. Neither isothermal or constant heat flux models are sufficiently accurate to obtain the observed flow structures. The flow configuration with two interacting cold and warm counter-rotating circulations appears to be very sensitive to the changes of the heat flux through the passive walls. Direct comparison of the numerical and experimental results is necessary to verify assumptions made when building a new model. Hence, the side walls were incorporated into the computational domain in the new fixed grid model (FGM). Figure 7 shows two results of the numerical simulations obtained using the FGM code for a 41^2 mesh, and with both adiabatic TBC and non-adiabatic 2D-TBC (conjugate heat transfer model). The heat transfer coefficient for the external walls was chosen at 20 W/Km^2, which corresponds to the typical experimental conditions. This is in very good agreement with the experimental observations.

We may conclude that solving the coupled solid–fluid heat conduction problem together with the Navier–Stokes equations improves the modelling of the flow pattern. But still empirical values for the air-wall heat flux coefficients have to be used to close the model.

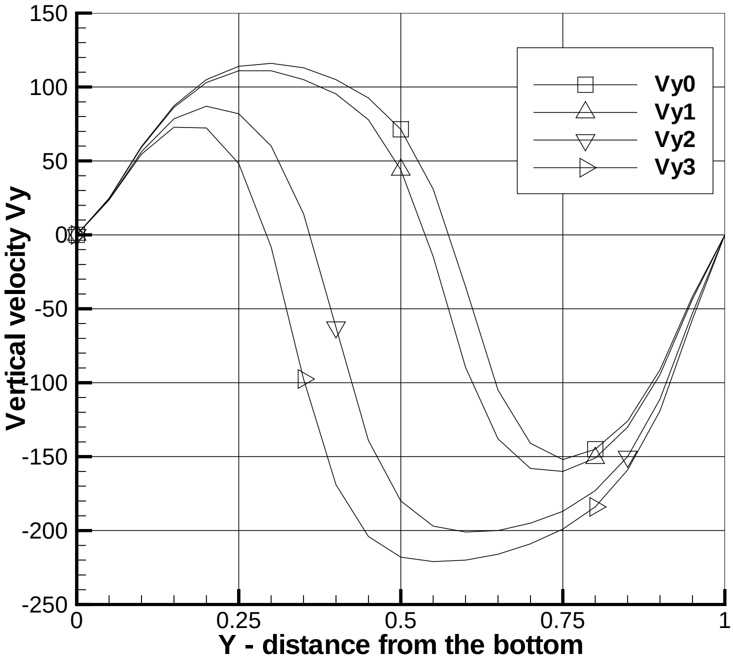

Fig. 6. Natural convection of water, vertical velocity profiles calculated close to the cold wall: vertical line at $x = 0.93$, $z = 0.5$ (3D calculations). Effect of the heat flux through the side walls: Vy0 – adiabatic, Vy1 – $h = 2W/Km^2$, Vy2 – $h = 20W/Km^2$, Vy3 – $h = 40W/Km^2$. Zero crossing of the profiles indicates position of the saddle point of the colliding hot–cold circulations

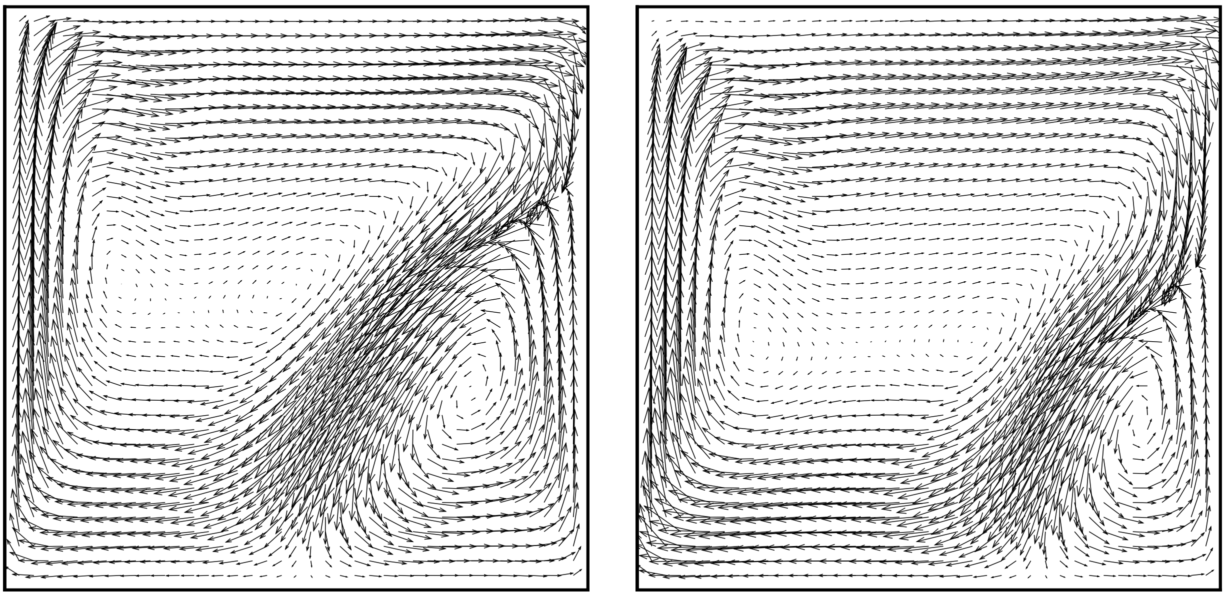

Fig. 7. Natural convection of water, $T_h = 10°C$, $T_c = 0°C$. FGM 2D solution: (left) – adiabatic boundary conditions, (right) – non-adiabatic 2D TBC (conjugate heat transfer model)

7. Freezing of water

7.1. Experimental observations

The pure convection experiments show, as already mentioned, two main circulation regions. The first, driven by normal convection, is located in the upper part of the cavity. It transports the hot liquid up to the top wall and back along the isotherm of the density extreme. The freezing experiments are conducted by starting from the steady natural convection and changing the cold wall temperature from 0°C to −10°C. When the freezing starts from the developed flow, the fluid/solid interface remains at the isothermal temperature 0°C. However, interaction of the convective flow with the freezing front causes deformation of the initially flat freezing plane (see Fig. 8). The hot circulation melts the upper parts of the ice front, reducing the ice growth rate in this region. The abnormal flow circulation, located in the lower right part of the cavity, transports the cold liquid up along the adjacent ice surface and back to the bottom along the isotherm of the density extremum. This cold water circulation only moderately modifies the heat balance at the interface. The convective heat transfer between both upper and lower regions seems to be limited mainly to the upper right corner of the cavity. There, along the colliding cold and warm fluid layers, the heat is transferred from the hot wall to the lower parts of the cavity. The shape of the freezing front reproduces this interaction, almost doubling the ice growth rate at the bottom. It can be seen in Fig. 9, which shows the measured velocity field and the ice front position for the several time steps during the freezing experiment.

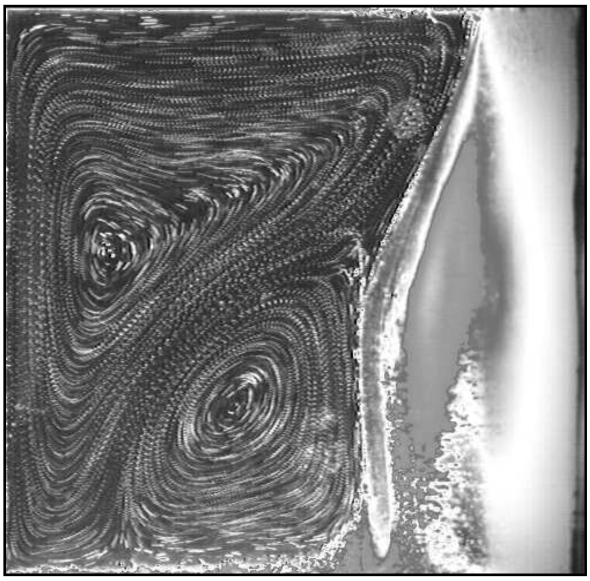

Fig. 8. Flow structure and ice front observed for the centre plane ($z = 0.5$) at 2600 s after freezing starts

7.2. Vorticity-vector potential transformed grid model

The transformed grid model (ICE3D) described above was used to run a large number of cases to illustrate previously reported [2, 19] discrepancies appearing between the numerical simulations and the experimental data. Our main concern was to model correctly the thermal boundary conditions at the side walls. Three different approaches were investigated: adiabatic side walls, heat flux through the side wall (1-D TBC) and the conjugate heat flux model (3-D TBC). When non-adiabatic conditions are used, the heat transfer coefficient for the air – cavity heat flux was estimated to be 20 W/Km^2.

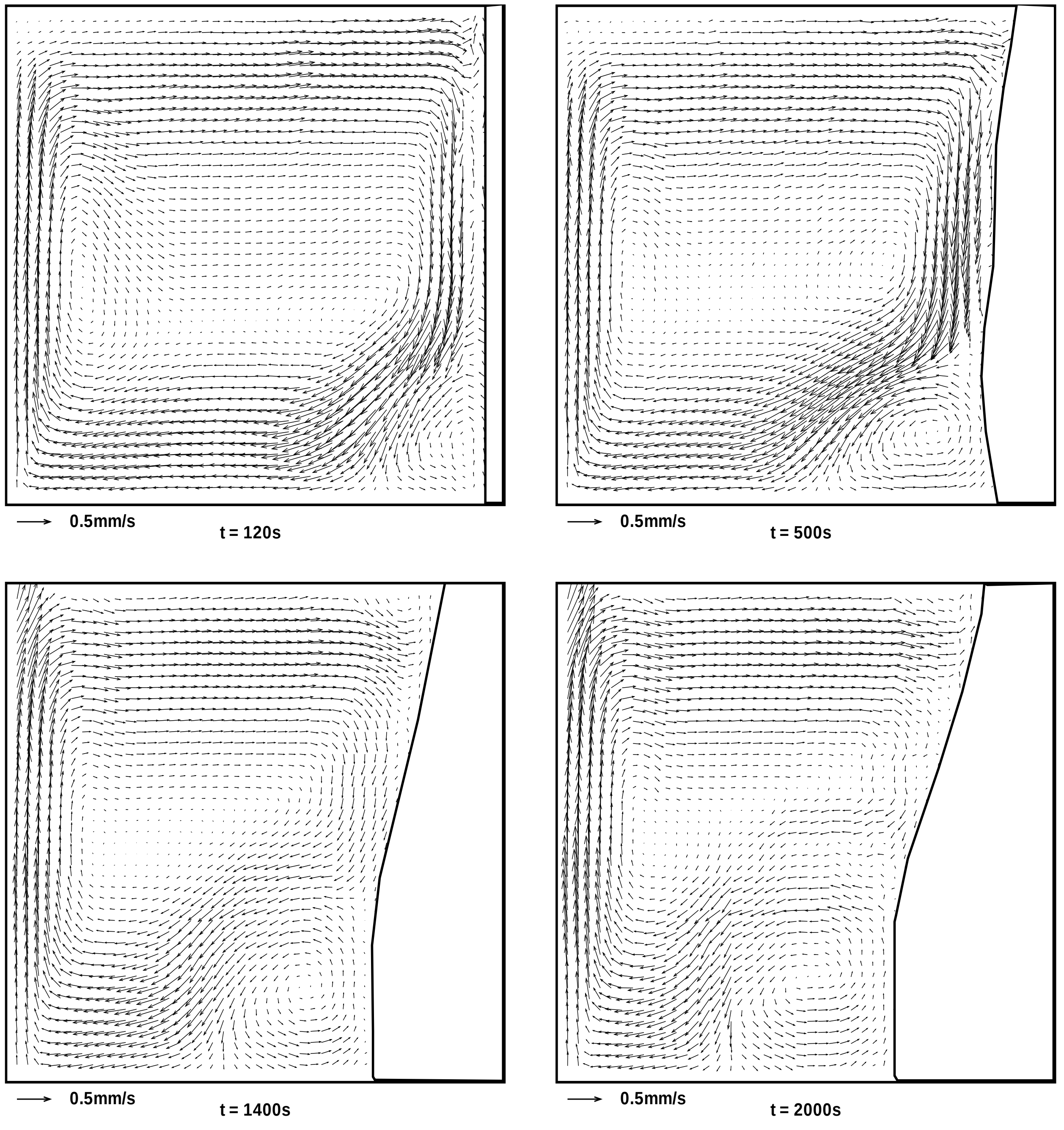

Fig. 9. Measured velocity field at 120 s, 500 s, 1400 s, and 2000 s after freezing process starts from the steady convective flow; $T_h = 10°C$, $T_c = -10°C$

Solutions were obtained using 31^3 mesh points for the fluid and 31x31x10 additional mesh points for the solid. Using the 3-D TBC five additional grid points were located in each of the four side walls. To test the mesh dependence the selected cases were calculated increasing the number of grid points to 61^3 for the fluid domain. To start the freezing calculations an initial grid for the solid phase must exist. Hence, it was assumed that at the first instant the cold wall is already covered with an ice layer of a non-dimensional thickness of 0.02. The freezing calculations start, as described above, when the steady state solution for the natural convection is established. Using the ICE3D numerical model all necessary details about the three-dimensional flow structure are obtained.

The effect of modelling TBC on the flow structure is illustrated in Fig. 10. The temperature and velocity fields are displayed for the centre vertical plane and close to the side wall for the time step 500s after freezing starts. For the 3D-TBC the temperature field at the external surface of the front wall is also shown.

Calculations obtained for the adiabatic walls (Fig. 10a), have been repeated assuming one dimensional heat flux from the surrounding air (1-D TBC) through the side walls (Fig. 10b), or by including the side walls in the computational domain (Fig. 10c). It may be seen that the 1-D TBC approach compared with the adiabatic case generally modifies both the flow structure and the temperature field. The most advanced point of the interface moves down and the anti-clockwise circulation becomes smaller. The flow and temperature pattern are largely modified at the side wall compared with the adiabatic case. The upper part of the ice layer is thinner, the lower part exhibits a characteristic inclination before touching the bottom wall (see left subfigure of Fig. 10b). These reasonably resemble the experimental observations.

Compared to the 1-D TBC results the 3-D modelling of the TBC (Fig. 10c) shows rather small change for the ice shape and the flow pattern in the centre cross section. Some further differences between both non-adiabatic cases are visible for the plane close to the front wall. The effect of the heat flux thorough this wall can be seen for the isotherms calculated for the external surface of the wall. We were able to confirm such variation of the isotherms at the external walls by employing infrared thermography [30].

It was found that there is relatively good agreement between the numerical simulations and the experiments at the initial stages of the freezing process (Fig. 8). However, it is not the case for longer freezing times. Despite our improvements in the modelling and even dramatic increase of the mesh resolution (61^3), the already reported discrepancies [19] in the ice front are more and more pronounced when the freezing time exceeds 500 s.

7.3. Vorticity–velocity fixed grid numerical model

The fixed grid enthalpy–porosity model described above was used to generate solutions for the freezing of water. To reduce computational time only a two-dimensional problem was solved. Our mesh refinement reported above convinced us to select a 41^2 mesh for the fluid domain as a good compromise between the accuracy and the time of calculations. The solutions are obtained starting, as it was described above, from the developed natural convection as an initial condition. Both adiabatic and 2-D TBC were implemented to study their effect on the solution accuracy. It was found that incorporation of the non-isothermal walls (i.e. the top and bottom walls for our 2-D problem), into the computational domain improves the final solution. Both the shape of the ice front and the flow structure are very close to that observed in the experiments (see Fig. 11). However, as before, differences progressively developed as the interface grew. Especially the lower parts of the ice front suffered evident errors in modelling when the freezing time exceeds 1000 s. In the experiments the ice surface remains almost perpendicular to the bottom wall, whereas in the numerical results for large time its shape receded back towards the cold wall. It seems that the numerical modelling of counter-clockwise circulation at the lower parts leads to an overestimate of the heat flux in this region. This decreases the ice growth at the low parts of the cavity.

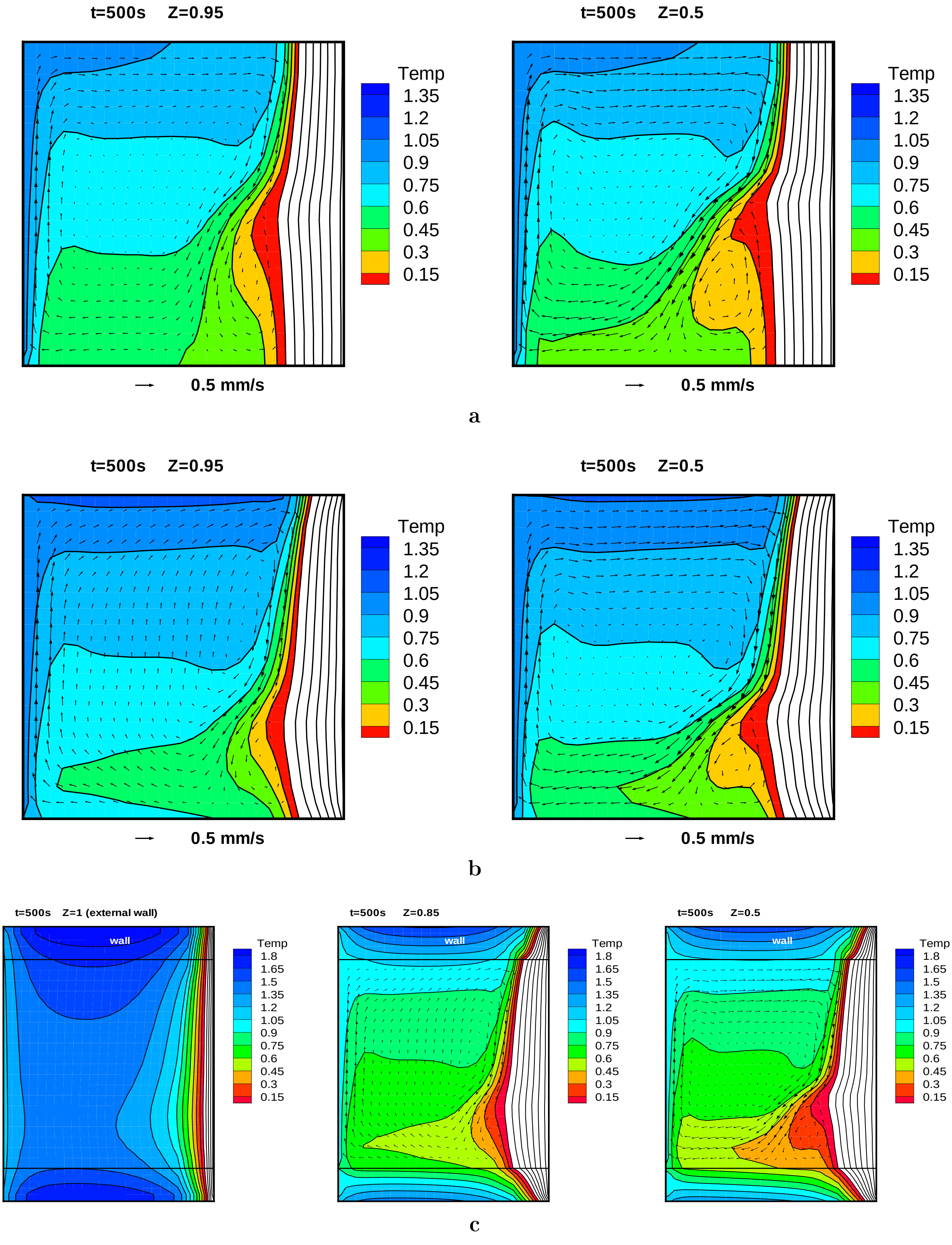

Fig. 10. Temperature and velocity fields at 500 s after freezing starts, calculated (ICE3D) for three types of thermal boundary conditions: adiabatic (a), non-adiabatic 1-TBC (b), non-adiabatic 3-TBD (c). Vertical cross-section at the side wall (left) and centre plane (right); $T_h = 10°\mathrm{C}$, $T_c = -10°\mathrm{C}$

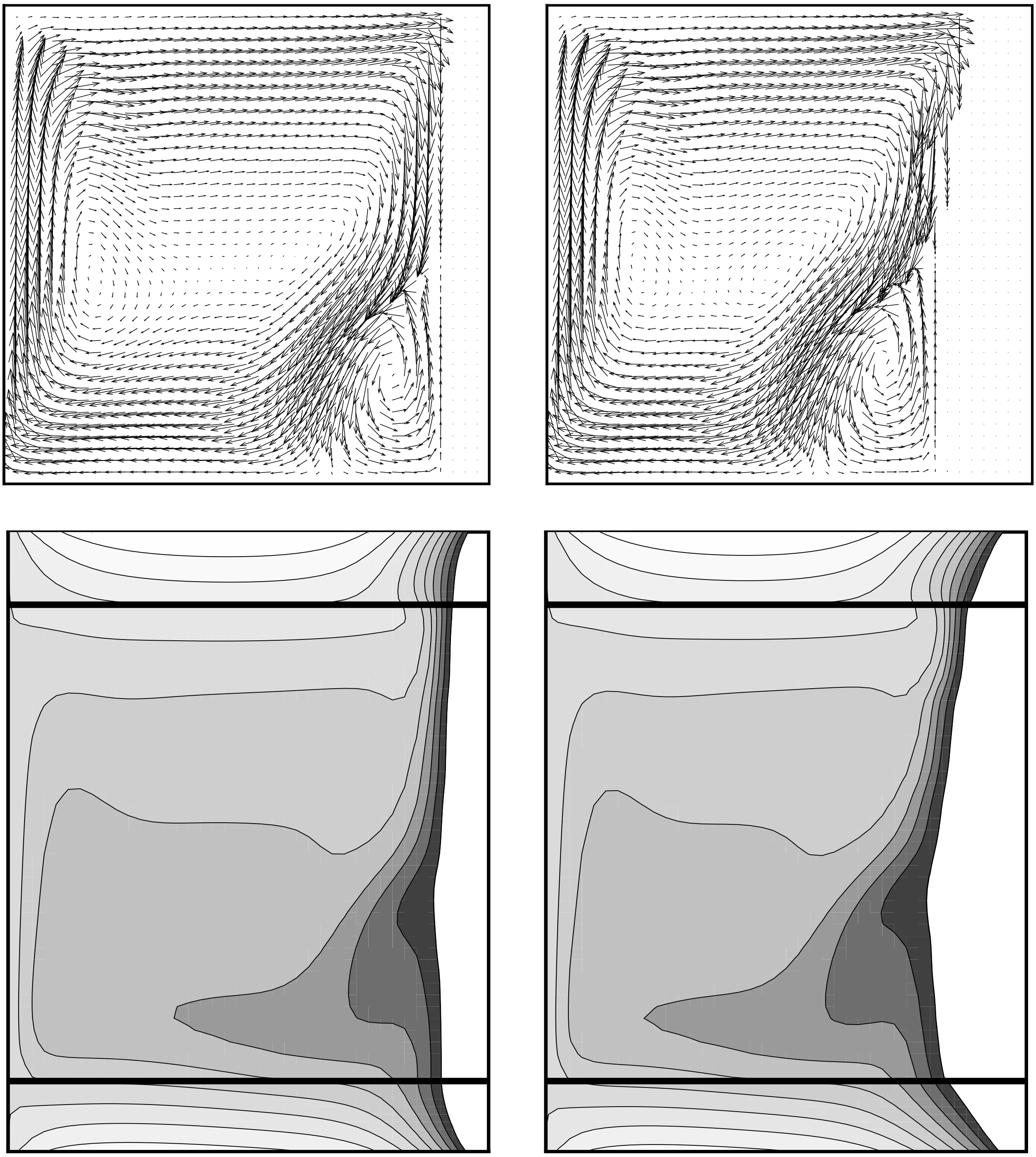

Fig. 11. Freezing of water: $T_h = 10°C$, $T_c = -10°C$. Numerical solutions (FGM) obtained at 120's (left column) and 500's (right) after freezing starts from the steady convective flow. Velocity vectors (top row) and temperature fields (bottom) displayed

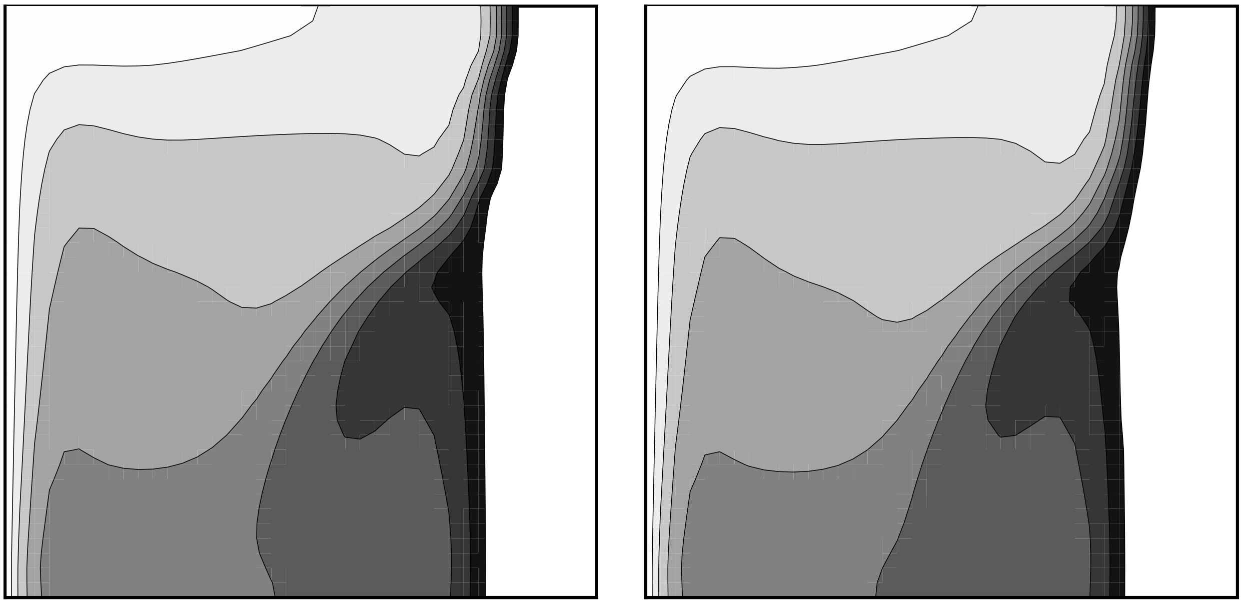

Fig. 12. Freezing of water for $T_h = 10°\text{C}$, $T_c = -10°\text{C}$, flow field calculated for adiabatic boundary condition. Numerical solutions (FGM) obtained at 500 s after freezing starts from the steady convective flow; left: single mesh; right: double mesh

In the fixed grid model the phase change surface does not appear explicitly in the solution. The shape of the ice front is obtained by interpolating for the 0°C isotherm at the relatively coarse grid points. Hence, it may exhibit non-physical shape oscillations, especially visible when the surface deformation increases (see the 500 s time step in Fig. 11b). For freezing water the temperature field and the liquid fraction are crucial for proper evaluation of the phase change interface. The inaccuracy of this evaluation may to some extend be responsible for accumulation of errors in time for the energy balance at the interface. To verify this, the new two-mesh version of the code was used. Hence, the energy equation was solved on a refined grid (161×161), while the momentum equation on a coarse mesh (41×41). It can be seen that our approach based on two different grids for energy and momentum equation smoothes the solidification front (see Fig. 12) removing most of the characteristic wiggles. However, the overall structure of the flow remained the same, when the freezing time increased.

The present improved fixed grid method exhibits all the advantages of a transformed grid method, but at a much lower computational cost. However, the problem with discrepancies between the experimental and numerical results for the long time runs still remains.

8. Conclusions

We hope that the results presented here at least partly elucidate problems with the numerical modelling of the complex flow structures for natural convection of water in the vicinity of the freezing point. The importance of properly incorporating the thermal boundary conditions on the passive walls is clearly demonstrated. It is necessary that the thermal conditions at these walls are sufficiently well described by the experimental procedure. As we have shown, a small variation of the heat flux or temperature leads to significant variations to the flow pattern. Very good mesh resolution is also essential.

When freezing starts, good agreement between numerical and experimental results could be achieved for initial time of the transient process. The agreement progressively decreases for longer experimental time. One of possible reasons could be inappropriate modelling of the thermal properties of ice. It is well known that ice consists of water and air trapped during the freezing time. Non-uniformity of the ice structure, dendrites, and impurities due to the dissolved gases may force us to modify the assumption used about isotropy of the thermal properties of the ice. Also the morphological structure of ice may vary, depending on the physics of the freezing process [5].

Another important point is the analysis of the effects of supercooling. Most of the investigations concerning solidification assume isothermal conditions at the phase change boundary and temperatures above the freezing point for the liquid phase. However, it is well known that usually fluid supercooling precedes the phase change [13]. For example, we observed in the experiments that water of standard purity will supercool to about $-5°C$ to $-7°C$, before ice nucleation appears. This may significantly retard the solidification process, modifying initial flow pattern. Thus, an understanding of the role of supercooling in the solidification process is required.

Acknowledgements

We gratefully acknowledge CIRA S.c.p.A. (Centro Italiano Ricerche Aerospaziali) for the use of the POWER CHALLENGE supercomputer. The second author acknowledge research grant no. PB580 T099712 of KBN (State Committee for Scientific Research) and the access to CRAY-CS6400 computer granted by the Warsaw University of Technology (COI).

References

[1] C. Abegg, G. de Vahl Davis, W.J. Hiller, St. Koch, T.A. Kowalewski, E. Leonardi, G.H. Yeoh. Experimental and numerical study of three-dimensional natural convection and freezing in water. *Heat Transfer*, **4**: 1–6, IchemE, Taylor & Francis, London, 1994.

[2] J. Banaszek, M. Rebow, T.A. Kowalewski. Fixed grid finite element analysis of solidification. In: G. de Vahl Davis, E. Leonardi, eds., *Advances in Computational Heat Transfer*, 471–478. Begel House Inc., New York, 1998.

[3] J. Banaszek, Y. Jaluria, T.A. Kowalewski, M. Rebow. Semi-implicit FEM analysis of natural convection in freezing water. *Num. Heat Transfer*, Part A, **36**: 449–472, 1999.

[4] O. Bertrand, B. Binet, H. Combeau, S. Coutier, Y. Delannoy, D. Gobin, M. Lacroix, P. Le Quéré, M. Médale, J. Menciger, H. Sadat, G. Vieira. Melting driven by natural convection. A comparision exercise: first results. *Int. J. Therm Sci.*, **38**: 5–26, 1999.

[5] K.C. Cheng, Y.C. Yen. Historical and recent developments in the research of cold regions heat transfer. In: *Proc. of 2nd Int. Symp. Cold Regions Heat Transfer*, 1–25, 1989.

[6] S. Fukusako, M. Yamada. Recent advances in research on water-freezing and ice-melting problems. *Exp. Therm. Fluid Scs.,* **6**: 90–105, 1993.

[7] C. Gau, R. Viskanta. Flow visualization during solid–liquid phase change heat transfer: Freezing in a rectangular cavity. *Int. Commun. Heat Mass Transfer,* **10**: 173–181, 1983

[8] M. Giangi. *Fenomeni di Convezione Naturale nei Processi di Solidificazione.* Ph. D. Thesis, University of Rome, La Sapienza, 1999.

[9] M. Giangi, F. Stella, T.A. Kowalewski. Numerical simulation of natural convection during ice formation. In: *IV Congresso nazionale della società italiana di matematica applicata ed industriale.* (Simai), 1–5 giugno 1998.

[10] M. Giangi, F. Stella, T.A. Kowalewski. Phase change with free convection: fixed grid simulation. *Comp. Visual. Scs.*, **2**(2/3): 123–130, 1999.

[11] W.J. Hiller, St. Koch, T.A. Kowalewski, F. Stella. Onset of natural convection in a cube. *Int. J. Heat Mass Transfer*, **36**: 3251–3263, 1993.

[12] F. Kohlrausch. *Praktische Physik*, Band 3, 22 Auflage, Table 22203. B.G. Teubner Stuttgart, 1.692–1.693, 1968.

[13] C.A. Knight. *The freezing of supercooled liquids.* D. Van Nostrand Co., Toronto, 1967

[14] T.A. Kowalewski. Experimental validation of numerical codes in thermally driven flows. In: G. de Vahl Davis, E. Leonardi, eds., *Advances in Computational Heat Transfer*, 1–15. Begel House Inc., New York, 1998.

[15] T.A. Kowalewski, A. Cybulski. Experimental and numerical investigations of natural convection in freezing water. *Int. Conf. on Heat Transfer with Change of Phase*, Kielce. In: *Mechanics*, **61**(2): 7–16, 1996.

[16] T.A. Kowalewski, A. Cybulski. Natural convection with phase change (in polish). *IFTR Reports* 8/1997, IPPT PAN, Warszawa, 1997.

[17] T.A. Kowalewski, A. Cybulski, M. Rebow. Particle image velocimetry and thermometry in freezing water. In: G.M. Carlomagno, I. Grant, eds., *8th Int. Symposium on Flow Visualization*, Sorrento. CD ROM Proceedings ISBN 0953399109, 24.1–24.8, Edinburgh, 1998.

[18] T.A. Kowalewski, M. Rebow. An experimental benchmark for freezing water in the cubic cavity. In: G. de Vahl Davis, E. Leonardi, eds., *Advances in Computational Heat Transfer*, 149–156. Begel House Inc., New York, 1998.

[19] T.A. Kowalewski, M. Rebow. Freezing of water in the differentially heated cubic cavity. *Int. J. of Comp. Fluid Dyn.*, **11**: 193–210, 1999.

[20] E. Leonardi, J.A. Reizes. Convective flows in closed cavities with variable fluid properties. In: R.W. Lewis *et al.*, eds., *Numerical Methods in Heat Transfer*, 387–412. John Wiley & Sons, 1981.

[21] E. Leonardi, T.A. Kowalewski, V. Timchenko, G. de Vahl Davis. Effect of finite wall conductivity on flow structures in natural convection. In: A.A. Mohamad, I. Sezai, eds., *Proceedings of the International Conference on Computational Heat and Mass Transfer CHMT99*, 182–188. Eastern Mediterranean University Printinghouse, Cyprus 1999.

[22] P. Le Quéré, D. Gobin. A note on possible flow instabilities in melting from the side. *Int. J. Therm Sci.* **38**: 595–600, 1999.

[23] D.S. Lin, M.W. Nansteel. Natural convection heat transfer in a square enclosure containing water near its density maximum. *Int. J. Heat Mass Transfer*, **30**: 2319–2329, 1987.

[24] G.D. Mallinson, G. de Vahl Davis. Three-dimensional natural convection in a box: a numerical study. *J. Fluid Mech.,* **83**: 1–31, 1977.

[25] N. Ramachandran, J.P. Gupta, Y. Jaluria. Thermal and fluid flow effects during solidification in a rectangular enclosure. *Int. J. Heat Mass Transfer*, **25**: 187–194, 1982.

[26] J.A. Reizes, E. Leonardi, G. de Vahl Davis. Natural convection near the density extremum of water. In: *Proc. of Fourth Int. Conf. on Numerical Methods in Laminar and Turbulent Flow*, Swansea, U.K., 794–804, 1985.

[27] L. Robillard, P. Vasseur. Transient natural convection heat transfer of water with maximum density effect and supercooling. *Trans. ASME*, **103**: 528–534, 1981.

[28] J.C. Slattery. *Momentum Energy and Mass Transfer in Continua.* Kieger, New York, 1987.

[29] V. Tmichenko, E. Leonardi, G. de Vahl Davis. *FRECON3V Users' Manual.* The UNSW Report 1997/FMT/1, Sydney, 1997.

[30] T. Wiśniewski, T.A. Kowalewski, M. Rebow. Infrared and Liquid Crystal Thermography in Natural Convection. In: G.M. Carlomagno, I. Grant, eds., *8th Int. Symposium on Flow Visualization*, Sorrento. CD ROM Proceedings ISBN 0953399109, 212.1–212.8, Edinburgh, 1998.

[31] H. Van De Worst. A fast and smoothly converging variant of Bi-Cgstab for the solution of non-symmetric linear systems. SIAM, *J. Sci. Stat. Comput.*, **132**: 631–644, 1992.

[32] R. Viswanath, Y. Jaluria. A comparison of different solution methodologies for melting and solidification problesm in enclosures. *Num. Heat Transfer*, B **24**: 77–105, 1993.

[33] V.R. Voller, Cross M. and N.C. Markatos. An enthalpy method for convection–diffusion phase change. *Int. J. Num. Meth. Eng.*, **24**: 271–284, 1987.

[34] G.H. Yeoh. *Natural Convection in a Solidifying Liquid.* Ph.D. Thesis. The University of New South Wales, 1993.

[35] G.H. Yeoh, M. Behnia, G. de Vahl Davis, E. Leonardi. A numerical study of three-dimensional natural convection during freezing of water. *Int. J. Num. Meth. Eng.*, **30**: 899–914, 1990.